RSC Advances

ROYAL SOCIETY OF CHEMISTRY

www.rsc.org/advances

Graphical Abstract

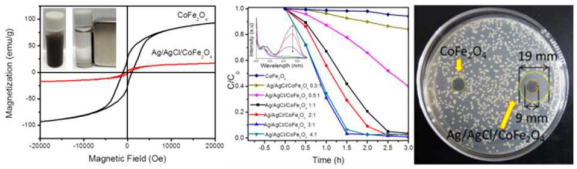

The magnetic separable $Ag/AgCl/CoFe_2O_4$ photocatalyst possess high photocatalytic ability and antibacterial ability.

Journal Name

RSCPublishing

ARTICLE

Preparation of magnetic Ag/AgCl/$CoFe_2O_4$ with high photocatalytic and antibacterial ability

Cite this: DOI: 10.1039/x0xx00000x

Yuanguo Xu,[a,b] Teng Zhou,[a] Shuquan Huang,[a] Meng Xie,[c] Hongping Li,[a] Hui Xu*,[a] Jiexiang Xia,[a] Huaming Li*[a]

Received 00th January 2012,
Accepted 00th January 2012

DOI: 10.1039/x0xx00000x

www.rsc.org/

The novel plasmonic photocatalysts Ag/AgCl/$CoFe_2O_4$ were first prepared via a two-step synthesis method. The obtained Ag/AgCl/$CoFe_2O_4$ composites were characterized by X-ray diffraction (XRD), transmission electron microscopy (TEM), X-ray photoelectron spectra (XPS) and ultraviolet-visible absorption spectra (UV-vis). The magnetic properties of the samples were studied by vibrating sample magnetometer (VSM) analysis. The methyl orange (MO), bisphenol A (BPA) and ciprofloxacin (CIP) were used as the target pollutants to investigate the degradation capability of Ag/AgCl/$CoFe_2O_4$. The results showed that the composite can degrade both color and colorless pollutants, while the Ag/AgCl/$CoFe_2O_4$ (3 : 1) showed the highest photoactivity in degrading MO. It can degrade about 93.38 % MO in 1.5 h. The reactive species scavenger results indicated that the hydroxyl radicals (•OH) was not the main photooxidant, while holes (h^+) and superoxide anion radicals ($\bullet O_2^-$) played key roles in MO decoloration. Furthermore, the degraded solution of BPA was analyzed by the High Performance Liquid Chromatography (HPLC). The results showed the BPA was decomposed gradually. The composite was magnetic separated and investigated by three successive recycle experiments under visible light. The result exhibited the photoactivity of Ag/AgCl/$CoFe_2O_4$ is stable. Besides, Ag/AgCl/$CoFe_2O_4$ also exhibited good antibacterial activity against *Escherichia coli* (*E. coli*). The preparation method can be expanded to apply to other magnetic separable photocatalyst.

Keywords: Ag/AgCl, $CoFe_2O_4$, photocatalyst, degradation, Ag/AgCl/$CoFe_2O_4$, antibacterial

Introduction,

Nowadays, with the development of modern industry, the environmental problems become even serious and have attracted more and more attentions. Water pollution is one of the serious issues among all of them which need to be highly noticed, because the clean water is a necessity for us. Lots of water sources are polluted not only by the hazardous chemicals but also by pathogenic microorganisms [1]. Pathogenic bacteria in water will cause diseases. Among many solutions, semiconductor-based photocatalysis technique is an efficient and low-cost strategy for the treatment of water pollutants and disinfection [2]. In recent years, the visible-light response plasmonic photocatalysts have attracted extensive research attention due to the surface plasmon resonance (SPR) effect [3]. In general, the photocatalysts with the surface plasmon resonance (SPR) effect have excellent absorption property in the visible light region and can efficiently separate the photogenerated electrons and holes, which is benefit for the photocatalytic degradation reactions. Besides, the Ag related materials have excellent antibacterial ability [4, 5]. The plasmonic photocatalysts based on silver/silver halide (Ag/AgX, X=Cl, Br) have attracted wide attention due to their extraordinary high photoactivity. Amount of works have been reported for the preparation of Ag/AgX (X=Cl, Br). For example, Huang et al. has fabricated a series of Ag@AgX (X = Cl, Br) plasmonic photocatalysts [6,7], which exhibited excellent photoactivity and stability under visible-light illumination. In the silver halide systems, AgX is the main photoactive species. However, pure AgX is instable under sunlight due to their photosensitive property [6,8,9]. Furthermore, when a certain amount of Ag (0) nanoparticles was reduced on the surface of AgX, the metallic Ag (0) could suppress the further decomposition of AgX. Therefore, Ag/AgX is a photo stable photocatalyst with high visible light photoactivity [10-16]. Besides, Ag/AgX can also disperse on other materials to improve the photoactivity of the composite [17-19]. Ag/AgX (Cl, Br) have become a serial of very important photocatalyst and they are playing an increasingly important role on solving the water pollutant problems. Lots of relevant works have also been used in antibacterial (such as Ag/AgCl/$W_{18}O_{49}$, Ag/AgBr/TiO_2, Ag/AgX/CNTs and so on). The Ag/AgX system showed very high antibacterial ability under light irradiation because it can efficiently generate reactive species to kill the bacterial [1, 5]. However, Ag/AgX photocatalysts also face the difficulty of being separated after the photocatalytic reaction, which limited its application in practical fields. To solve this problem, Ag/AgX was combined with magnetic material. Dai et al. [20] prepared core-shell Fe_3O_4@SiO_2 NPs at first, and then fabricated Ag-AgI/Fe_3O_4@SiO_2 plasmonic photocatalyst. The composite showed excellent photocatalytic activity and possess the capability of being easily recovered by magnet. Soon afterwards, An et al. [21] constructed Fe_3O_4@SiO_2 nanospheres through a polyol and sol-gel process at first, and then fabricated ferromagnetic Fe_3O_4@SiO_2@AgCl:Ag plasmonic nanophotocatalysts. The composite exhibited excellent

performance in the decomposition of rhodamine B (RhB) under visible-light irradiation. Besides, this catalyst can be separated easily by applying an external magnetic field. Tian et al. [22] synthesized core-shell structured γ-Fe_2O_3@SiO_2@AgBr:Ag composite by a versatile multistep route. They fabricated magnetic core firstly, and then coated SiO_2 interlayer. After that, they deposited AgBr shell. At last, the AgBr was reduced to form Ag nanoparticles on its surface by light irradiation. This photocatalyst exhibited very high photocatalytic activity and good magnetic property. All these strategies have achieved great advantages in developing magnetic plasmonic nanophotocatalysts. However, as we all know, either Fe_3O_4 or γ-Fe_2O_3 is not the ultimate stable crystal structure iron oxide. They both face the risk of conversion. The introduction of SiO_2 shell can solve the problem. However, the synthesis route could become cumbersome. Thus, discovery of a stable magnetic material and facile synthesis route is vital.

Spinel $CoFe_2O_4$ nanoparticle prepared by sol-gel method has excellent chemical stability, remarkable mechanical hardness and excellent magnetic property, which is a good choice for preparing semiconductor-magnetic composites. Some relevant works have been reported. Wang et al. [23] synthesized magnetic photocatalyst Bi_2WO_6/$CoFe_2O_4$ composites by a two-step hydrothermal method. This photocatalyst retained the effective photoactivity of Bi_2WO_6 and can be easily separated by the magnet. Ribeiro et al. [24] fabricated TiO_2/$CoFe_2O_4$ by the polymeric precursor method. The composite can degrade rhodamine B dye and atrazine pesticide under UV light irradiation and can be recovered by the magnet after the reaction. Phukan et al. [25] prepared $CoFe_2O_4$-ZnS magnetic composite. The composite showed good photoactivity in degrading methyl orange under UV irradiation and can be easily separated by a magnet. Besides, lots of other works have been reported, such as $CoFe_2O_4$/ZnO [26], $CoFe_2O_4$/TiO_2 [27] Pd(0)/SiO_2-$CoFe_2O_4$ [28], GO/$CoFe_2O_4$ [29]. In a world, $CoFe_2O_4$ is a promising magnetic material in fabricating magnetic photocatalysts.

Based on analysis above, it suggests that combining Ag/AgX and $CoFe_2O_4$ is a good propose, because it could lead to construct a new type magnetic plasmonic photocatalysts. In this work, $CoFe_2O_4$ was selected as a magnetic material to synthesize magnetic photocatalyst Ag/AgCl/$CoFe_2O_4$ composites by a facile solvothermal method. The as-prepared photocatalyst exhibited excellent degradation ability for methyl orange (MO), bisphenol A (BPA) and ciprofloxacin (CIP). Furthermore, this photocatalyst had a stable photoactivity and magnetic recoverable property. Besides, the composite showed good photocatalytic antibacterial ability against *Escherichia coli* (*E. coli*). This work may provide new insights in fabricating stable magnetic plasmonic photocatalysts by a facile method and expand the application of plasmonic photocatalysts in environmental remediation and water disinfection fields.

Experimental

2.1. Materials

All reagents were of analytical grade and were used without further purification.

2.2. Preparation of photocatalysts

2.2.1. Preparation of $CoFe_2O_4$

The $CoFe_2O_4$ sample was prepared according a reported method [30]: 10 mmol $Fe(NO_3)_3 \cdot 9H_2O$ and 5 mmol $Co(NO_3)_2 \cdot 6H_2O$ were dissolved in 100 mL distilled H_2O. The above solution was referred as solution A. Meanwhile, 15 mmol $C_6H_8O_7 \cdot H_2O$ was added into 100 mL distilled H_2O (referred as solution B). Then the solution A was added dropwise into the solution B under stirring and the temperature was kept at 60℃. After stirring for 1h, the mixture solution was moved to dryer and dried at 90℃ about 24 h. The obtained solid composite was then calcined at 400℃ and kept for 2 h.

2.2.2. Preparation of Ag/AgCl/$CoFe_2O_4$

The different mass ratios of $AgNO_3$ and $CoFe_2O_4$ (0.3:1, 0.5:1, 1:1, 2:1, 3:1, 4:1) were used to synthesize the Ag/AgCl/$CoFe_2O_4$ photocatalyst. Typically, the $AgNO_3$ and $CoFe_2O_4$ with the mass ratio of 3:1 were used as the example for the synthesis process, and the obtained Ag/AgCl/$CoFe_2O_4$ referred as Ag/AgCl/$CoFe_2O_4$ (3:1). Firstly, 0.0666g $CoFe_2O_4$ and 10 mL ethylene glycol solution of NaCl (0.0688 g) were mixed together and stirred for 30 min to form the homogeneous dispersion. Then 7 mL $AgNO_3$ EG solution (containing 0.2000 g $AgNO_3$) was added to the above homogeneous dispersion and stirred for 30 min at room temperature. After that, the resultant mixture was transferred to a Teflon lined autoclave and heated at 120℃ for 24 h. The resultant was centrifuged, washed and dried at 60℃ for 8 h. Similarly, other samples can be obtained with the addition of the appropriate amount of $CoFe_2O_4$.

2.3 Characterization

The crystal phase of the samples was analyzed by X-ray diffraction (XRD) analysis on the AdvantXP4200 (American) in the 2θ range of 10º-80º. Transmission electron microscopy (TEM) micrographs were taken with a JEOL-JEM-2010 (JEOL, Japan) operating at 200 kV. UV-vis absorption spectra of the liquid samples were taken on a UV-vis spectrophotometer (UV-2450, Shimadzu Corporation, Japan). The UV-vis absorption spectra of the solid samples (in the diffuse reflectance spectra mode) were measured in solid state, and $BaSO_4$ powder was used as the substrate. X-ray photoemission spectroscopy (XPS) was measured on a PHI5300 with a monochromatic Mg Kα source to explore the elements on the surface. The magnetic properties of the composites were tested in a vibrating sample magnetometer (VSM) (Quantum Design Corporation, USA) with a maximum applied field of ±2 T. High Performance Liquid Chromatography (HPLC) (LXQ Linear Ion Trap Mass Spectrometer) was used to analyze the degradation liquid. The HPLC setup was equipped with two Varian ProStar210 pumps, an Agilent TC-C (18) column, and a Varian ProStar325 UV-Vis Detector at 230 nm. A solution of methanol and H_2O in the ratio 75 : 25 (v/v) was used as the mobile phase with 1 mL min^{-1}. Then, 20 μL of the degraded solution was injected. The column oven temperature was 30℃.

2.4 Photocatalytic Activity

The application of the Ag/AgCl/$CoFe_2O_4$ composite in degrading organic dye methyl orange (MO) was investigated under visible-light irradiation at 30℃. In a typical procedure, a 0.0700 g samples was dispersed in 70 mL MO solution (10 mg/L). Until the lamp (300 W Xe arc lamp, with a cut-off filter supply visible light with $\lambda \geq 400$ nm) was turned on to start irradiation, the solution was stirred for 0.5 h in the dark to get the adsorption/desorption equilibrium between the photocatalyst and the dye. The solution was sampled at 0.5 h intervals and was centrifuged, and then the above liquid was monitored by UV-vis spectroscopy at 463 nm. The degradation of CIP and BPA was similar to the above operation. The degraded solution was analyzed by UV-vis spectrophotometer and HPLC.

2.5 Antibacterial activity

All of the glassware and the culture medium solution were sterilized by autoclaving at 121℃ for 20 min prior to use. All experiments were performed under sterile conditions.

The effect of sample on the bacterial growth in the absence of light was using qualitative test, inhibition zone (disc diffusion test). Firstly, 0.02 mL of the prepared *Escherichia coli (E. coli)* bacteria suspension was dispersed on nutrient agar medium. Then, about 9

mm diameter of the sample was prepared on the nutrient agar medium. At last, the culture dish was incubated at 37℃ for 24 h in dark.

The photocatalytic antibacterial experiments were performed in a typical method: 20 mg of as-prepared sample were added into 20 mL culture medium solution. Then, certain volume the prepared *Escherichia coli (E. coli)* bacteria suspension was transferred into the mixture (the mixture concentration is $1/(2*10^4)$ to that of original *E. coli*). The mixture was then magnetic stirred in the dark for 0.5 h, after that the light was open to start irradiation. 0.02 mL of the solution was sampled at the time of 0 min, 15 min and 30 min, respectively. Each solution was dispersed on nutrient agar medium and incubated at 37℃ for 24 h in dark.

Results and discussion,

3.1 XRD and TEM analysis

Fig.1 shows the XRD patterns of the magnetic photocatalyst $Ag/AgCl/CoFe_2O_4$ and pure $CoFe_2O_4$. As shown in Fig. 1a, the 2θ degree at 30.1°, 35.2°, 43.0°, 53.4°, 56.9° and 62.6° (marked with "♣") are correspond to the (220), (311), (222), (400), (422), (511) and (440) crystalline planes of the $CoFe_2O_4$ (JCPDS card no. 22-1086) [30], respectively. As shown in Fig. 1b, seven distinctive peaks at 32.1°, 46.2°, 54.7°, 57.4°, 67.4°, 74.4° and 76.6° (marked with "◆") were observed, which corresponding to the (200), (220), (311), (222), (400), (331) and (420) planes of AgCl crystal (JCPDS cards no. 31-1238) in the $Ag/AgCl/CoFe_2O_4$ (0.3:1). The distinctive peak at 38.1° (marked with "●") is ascribed to the (111) plane of metallic Ag (JCPDS cards no. 04-0783). Besides, no other diffraction peaks are found, which indicates that the composites are composed of Ag, AgCl and $CoFe_2O_4$. For further investigation of the composites of $Ag/AgCl/CoFe_2O_4$ photocatalyst, the $Ag/AgCl/CoFe_2O_4$ with different ratios were characterized and shown in Fig. 1 c-g. It can be seen that the intensity of the $CoFe_2O_4$ decreased gradually with the Ag/AgCl content increased, but the diffraction peaks of $CoFe_2O_4$ do not shift. It indicates that the addition Ag/AgCl was on $CoFe_2O_4$ surface, but not incorporated into its lattice.

The morphology of the pure $CoFe_2O_4$ and the $Ag/AgCl/CoFe_2O_4$ was investigated by TEM and the results are shown below. In Fig. 2A, it shows that the $CoFe_2O_4$ is in the form of small particles, which stick together and the average particles size is 20 nm approximately. Fig. 2B shows the TEM of $Ag/AgCl/CoFe_2O_4$ (3:1). The image reveals that several large particles (in the range of 50 nm-100 nm) are obviously different to that of $CoFe_2O_4$, which ascribed to the introduced Ag/AgCl. It can be seen that the Ag/AgCl particles and the $CoFe_2O_4$ particles stick together, which indicates that they have a good combination because they did not depart after the ultrasonic process before TEM analysis. The combination is beneficial to the magnetic separation of the $Ag/AgCl/CoFe_2O_4$ from the solution of contaminant. When the content of Ag/AgCl was raised ($Ag/AgCl/CoFe_2O_4$ (4:1)), the large particles become more in number and agglomerated together (as shown in Fig. 2 C). This may not beneficial to the photoactivity of the composite.

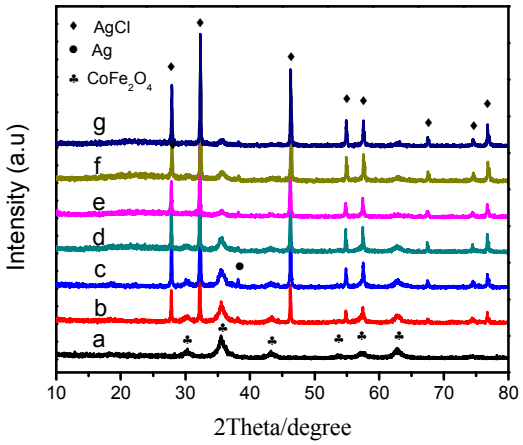

Fig.1 the XRD pattern of (a) $CoFe_2O_4$, (b) $Ag/AgCl/CoFe_2O_4$ (0.3:1), (c) $Ag/AgCl/CoFe_2O_4$ (0.5:1), (d) $Ag/AgCl/CoFe_2O_4$ (1:1), (e) $Ag/AgCl/CoFe_2O_4$ (2:1), (f) $Ag/AgCl/CoFe_2O_4$ (3:1) and (g) $Ag/AgCl/CoFe_2O_4$ (4:1).

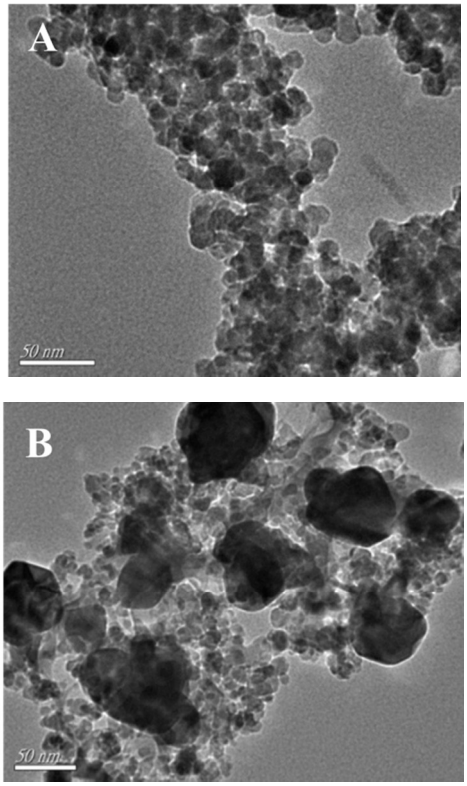

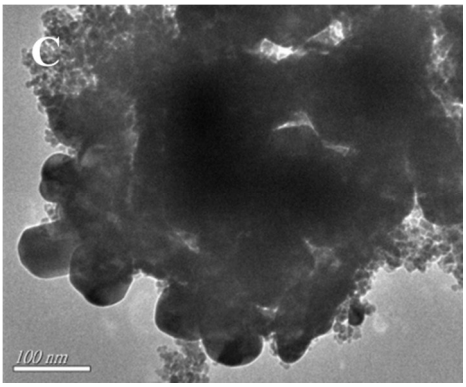

Fig. 2 TEM images of (A) $CoFe_2O_4$, (B) Ag/AgCl/$CoFe_2O_4$ (3:1) and (C) Ag/AgCl/$CoFe_2O_4$ (4:1).

3.2 XPS analysis

The XPS was used to measure the surface elements valences and components of the $CoFe_2O_4$ and Ag/AgCl/$CoFe_2O_4$. Fig. 3 A shows the survey spectrum of $CoFe_2O_4$ and Ag/AgCl/$CoFe_2O_4$ (3:1). It is obviously that the Ag/AgCl/$CoFe_2O_4$ (3:1) composite showed Ag 3d and Cl 2p signals more than that of $CoFe_2O_4$ (which possess O 1s, Co 2p and Fe 2p). Fig. 3 B, C, D and E show the high-resolution XPS spectrum of Co 2p, Fe 2p, Ag 3d and Cl 2p of the samples. As shown in Fig. 3 B, there're two peaks in the Co 2p spectrum for $CoFe_2O_4$, the peak at 795.3 eV corresponds to Co $2p_{1/2}$, while the peak at about 780.0 eV attributes to Co $2p_{3/2}$ [31]. When the Ag/AgCl was introduced, both the two peaks show a little shift. The peak at 795.3 eV shift to 795.9 eV and the peak at 780.0 eV shift to 780.5 eV. As shown in Fig. 3 C, the Fe 2p spectra possess two peaks at 711.0 eV (Fe $2p_{3/2}$) and 724.5 eV (Fe $2p_{1/2}$) suggesting the presence of Fe^{3+} cation [32]. Furthermore, these two peaks all shift after the deposition of Ag/AgCl (the peak at 711.0 eV shifts to 710.7 eV and the peak at 724.5 eV shift to724.0 eV.). The change of Co and Fe spectra indicate the addition of Ag/AgCl has combined with $CoFe_2O_4$ and affects the chemical condition of Co and Fe in $CoFe_2O_4$ sample. Fig. 3d shows the high-resolution spectrum of Ag 3d. The two peaks around 366.4 eV and 372.4 eV are ascribe to the $3d_{5/2}$ and $3d_{3/2}$ of Ag, respectively. Wherein, the two peaks both revealed a shift about 1 eV compared to pure Ag/AgCl to our previous work Ag@AgCl [33]. At the same time, for the Cl spectrum in Fig. 3E, the two peaks are observed at binding energy of about 196.7 eV and 198.3 eV, representing Cl $2p_{3/2}$ and Cl $2p_{1/2}$, respectively. Meanwhile, a shift of about 1 eV happened in the Cl 2p peak [33]. In all, the shift of Ag and Cl peaks reveal the chemical environment in the Ag/AgCl/$CoFe_2O_4$ sample has been changed when compared to pure Ag/AgCl. The XPS results disclosed the information of different kinds of element in Ag/AgCl/$CoFe_2O_4$ as well as proved the interaction between the Ag/AgCl and $CoFe_2O_4$. It suggests that the Ag/AgCl and $CoFe_2O_4$ has been successfully combined together instead of simple adsorption. Therefore, it would be beneficial to be separated by the external magnet.

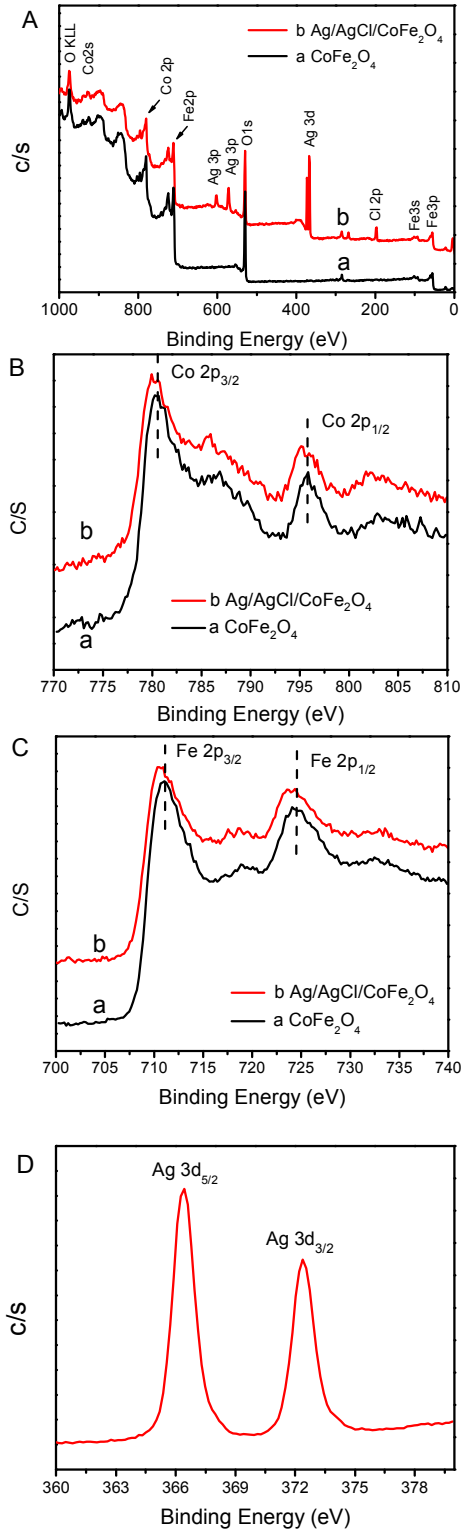

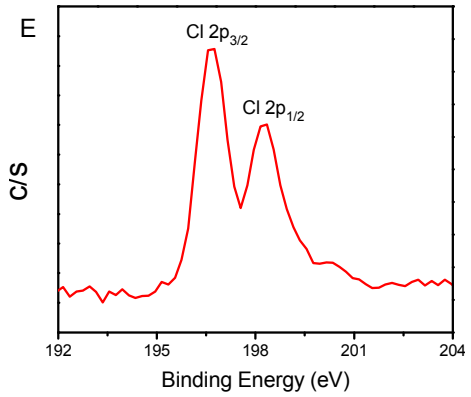

Fig. 3 The survey spectra of $CoFe_2O_4$, $Ag/AgCl/CoFe_2O_4$ (A) and the high resolution XPS spectrum of Co 2p (B), Fe 2p (C), Ag 3d (D) and Cl 2p (E).

3.3 UV-Vis analysis

The optical properties of the photocatalyst of $CoFe_2O_4$ and $Ag/AgCl/CoFe_2O_4$ composite were investigated by UV-vis absorption spectroscopy (in diffuse reflectance spectra (DRS) mode) and the results are shown in Fig. 4. As shown in Fig. 4a, the absorption intensity of pure $CoFe_2O_4$ is very high in both UV and visible light region. It may be due to the black color of the $CoFe_2O_4$ material. When Ag/AgCl was introduced, the absorption intensity of $Ag/AgCl/CoFe_2O_4$ composites decreased in UV and visible light region with the increase of Ag/AgCl content (as shown in Fig. 4 b-f). The higher content of Ag/AgCl leads to the lighter color of the composites. The phenomenon suggests that the introduced Ag/AgCl is covered on the surface of $CoFe_2O_4$.

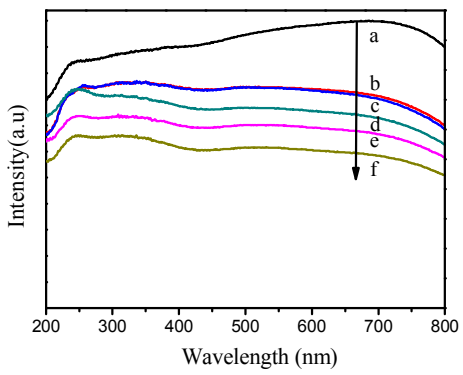

Fig. 4 UV-Vis absorption spectra of (a) $CoFe_2O_4$, (b) $Ag/AgCl/CoFe_2O_4$ (0.5:1), (c) $Ag/AgCl/CoFe_2O_4$ (1:1), (d) $Ag/AgCl/CoFe_2O_4$ (2:1), (e) $Ag/AgCl/CoFe_2O_4$ (3:1) and (f) $Ag/AgCl/CoFe_2O_4$ (4:1).

3.4 Magnetic performances

The magnetic property of the composites is very useful for the recovery of magnetic photocatalysts in solution reactions. The magnetic property of $CoFe_2O_4$ and $Ag/AgCl/CoFe_2O_4$ (3:1) was measured by the vibrating sample magnetometer (VSM). The magnetization measurements were carried out at room temperature and the applied magnetic field was 20 kOe. As Fig. 5 shows, the detected magnetic saturation (Ms) values of $CoFe_2O_4$ and $Ag/AgCl/CoFe_2O_4$ (3:1) are 93.4 emu/g and 17.2 emu/g, respectively. The coercivities of the two composites are nearly1003.1Oe and 351.1 Oe, and the remnant magnetizations (Mr) are 26.8 emu/g and 2.2 emu/g approximately for $CoFe_2O_4$ and $Ag/AgCl/CoFe_2O_4$ (3:1). Obviously, the above three properties of the $Ag/AgCl/CoFe_2O_4$ composite are lower than that of $CoFe_2O_4$. However, the magnetic property of $CoFe_2O_4$ in the composite was kept and can be used to separate the $Ag/AgCl/CoFe_2O_4$ (3:1) photocatalyst from reaction solution. The left inset photo displays the $Ag/AgCl/CoFe_2O_4$ (3:1) dispersed in solution. As shown in the right inset photo, the $Ag/AgCl/CoFe_2O_4$ (3:1) can be separated by an external magnet.

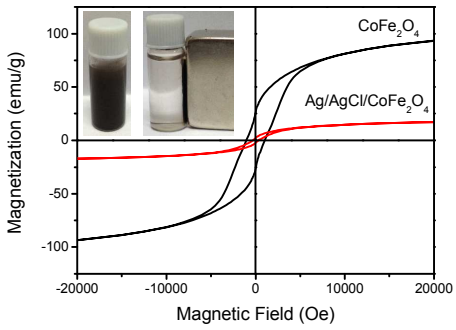

Fig. 5 Field-dependent magnetization curves of $CoFe_2O_4$ and $Ag/AgCl/CoFe_2O_4$ (3:1). The inset photos show the $Ag/AgCl/CoFe_2O_4$ (3:1) before and after magnetic separation.

3.5 Photocatalytic activity

Fig. 6 A illustrates the photocatalytic activity of the $CoFe_2O_4$ and $Ag/AgCl/CoFe_2O_4$ (with different Ag/AgCl content) for the degradation of MO in aqueous solution under visible-light irradiation. It is clear that the pure $CoFe_2O_4$ showed extremely low degradation efficiency for MO in 3 h. When the Ag/AgCl was introduced to combine with $CoFe_2O_4$, the degradation ability of $Ag/AgCl/CoFe_2O_4$ photocatalyst increased with the increasing content of the Ag/AgCl. The $Ag/AgCl/CoFe_2O_4$ (3:1) showed the highest photoactivity performance. It can decompose 93.38 % of MO in 1.5 h and 99.03 % in 3 h. Fig 6 B shows the full UV-vis spectra of MO during the photodegradation. It is clear that the intensity of the absorption peak at about 463 nm decreased gradually. It means the MO was gradually photodecomposed by the $Ag/AgCl/CoFe_2O_4$ (3:1) under visible-light irradiation. When the Ag/AgCl content was further raised, the $Ag/AgCl/CoFe_2O_4$ (4:1) degradation rate decreased compared to the $Ag/AgCl/CoFe_2O_4$ (3:1). It is probably because of the excessive AgCl agglomerate together (as shown in Fig. 2). The corresponding (C_0 - C) plot has a good linearity (Fig. 6 C), indicating that the sunlight-driven photodegradation of MO solutions in the presence of photocatalyst follows the zero-order kinetics. The degradation rate constant of MO is shown in Fig. 6 D. The degradation rate constant of $Ag/AgCl/CoFe_2O_4$ (3:1) is the highest. It indicates that it has the highest photoactivity, which is in good agreement with the Fig. 6 A.

It is known that a series of reactive species may be involved in the degradation process. In order to probe the underlying reactive species of the $Ag/AgCl/CoFe_2O_4$ during the photocatalytic process, some scavengers were used to investigate them. In this work,

isopropyl alcohol (IPA) was used as •OH scavenger, L-ascorbic acid was used as an $•O_2^-$ scavenger and disodium ethylenediaminetetraacetate (EDTA-2Na) was added as an h^+ scavenger. As shown in Fig. 6E, the introduction of isopropanol had little effect on the degradation efficiency. It indicates that the •OH was not the main dominant reactive species in this system. The degradation efficiency of MO was reduced significantly by the introduction of L-ascorbic acid (a quencher of $•O_2^-$) or EDTA-2Na (a quencher of h^+), suggesting that the $•O_2^-$ and h^+ played an important role in the photocatalytic degradation process. This is in good agreement with the reported work [34, 35].

Moreover, the photocatalytic stability of $Ag/AgCl/CoFe_2O_4$ was investigated by three repeated MO degradation experiments. As shown in Fig. 7, the photoactivity of the $Ag/AgCl/CoFe_2O_4$ (3:1) is still very high after three cycle experiments. The little decrease may be due to a loss of small amount photocatalyst in the recycle experiments. Therefore, $Ag/AgCl/CoFe_2O_4$ can be used as an effective, stable magnetic recoverable photocatalyst for organic compounds degradation.

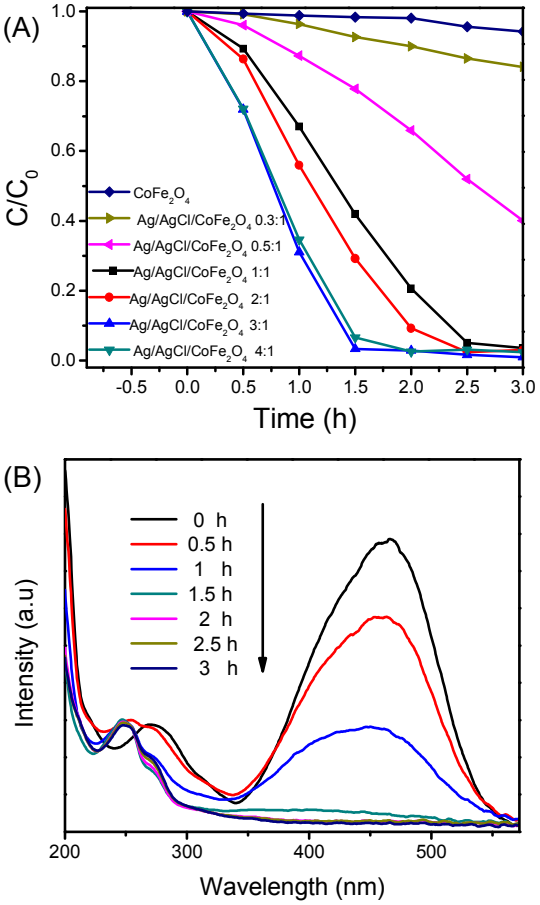

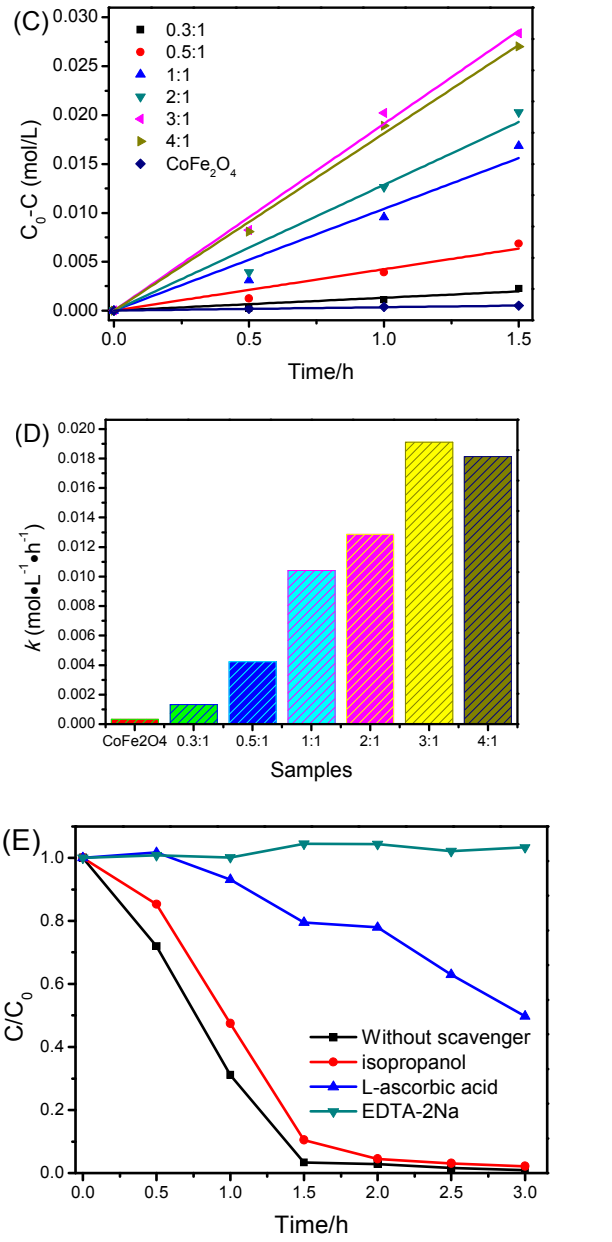

Fig. 6 The photoactivity of the samples in degrading MO dye under visible-light irradiation (A); the evolution of the absorption spectra of MO over time in the presence of $Ag/AgCl/CoFe_2O_4$ (3:1) (B), The zero-order kinetics of MO degradation in the presence of $CoFe_2O_4$ and $Ag/AgCl/CoFe_2O_4$ photocatalysts with different ratio of $Ag/AgCl:CoFe_2O_4$ (C); The degradation rate constant of MO with different samples(D) and the effects of some scavengers on the photocatalytic activity of the as-prepared $Ag/AgCl/CoFe_2O_4$ (3:1) for the photocatalytic decoloration of MO (E).

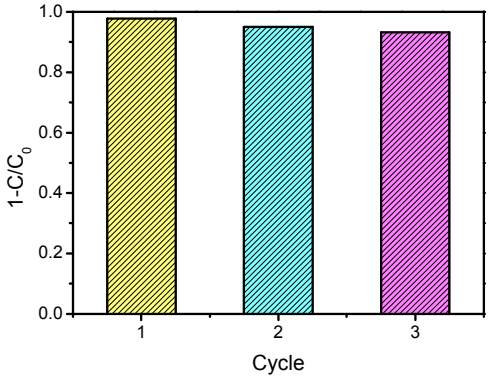

Fig. 7 The recycle experiments in the repeated MO degradation experiments with Ag/AgCl/$CoFe_2O_4$ (3:1) under visible-light irradiation.

As can be seen from the above results, Ag/AgCl/$CoFe_2O_4$ can degrade the color pollutant MO efficiently. In order to exclude the dye-sensitized reaction, the colorless pollutants of CIP and BPA were also used as the contaminants to further evaluate the mineralization ability of the Ag/AgCl/$CoFe_2O_4$ (3:1) composite. As shown in Fig. 8 A and D, it is clear that the CIP and BPA cannot be degraded under visible light irradiation without the existence of photocatalyst. The intensity of them show a little decreased after the $CoFe_2O_4$ was introduced, which may ascribed to some pollutant was adsorbed by the $CoFe_2O_4$ (as shown in Fig. 8 B and E). However, the pure $CoFe_2O_4$ has no photoactivity in degrading the CIP or BPA. The intensity of the pollutant did not decrease even after 3 h irradiation in the presence of $CoFe_2O_4$. As shown in Fig. 8 C, the two characteristic peaks of CIP decreased gradually. It suggests that the CIP can be efficiently degraded in the presence of Ag/AgCl/$CoFe_2O_4$ (3:1) under visible-light irradiation. Fig. 8 F shows the UV-vis absorption spectra of the aqueous solutions of BPA at different periods. It is clear that the characteristic peak of BPA decreased with the reaction time. Within 90 min reaction time, BPA was almost completely decomposed by Ag/AgCl/$CoFe_2O_4$ (3:1) photocatalyst. The degraded BPA solution was also investigated by the HPLC and the results are shown in Fig. 8 G. It is obviously that the characteristic peak of BPA decreased with the photoreaction process and almost disappeared in 90 min, which confirmed that the BPA was indeed decomposed by the Ag/AgCl/$CoFe_2O_4$ (3:1).

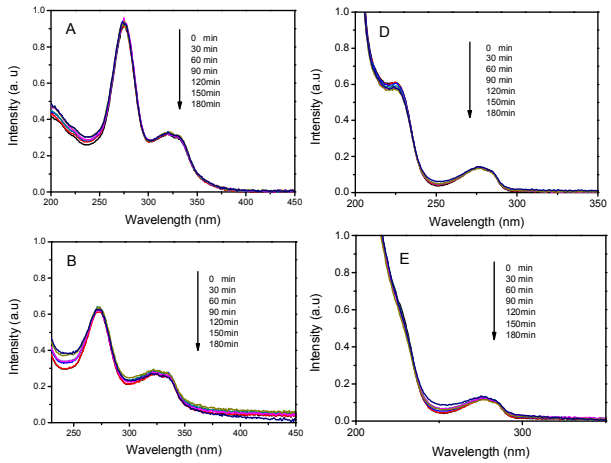

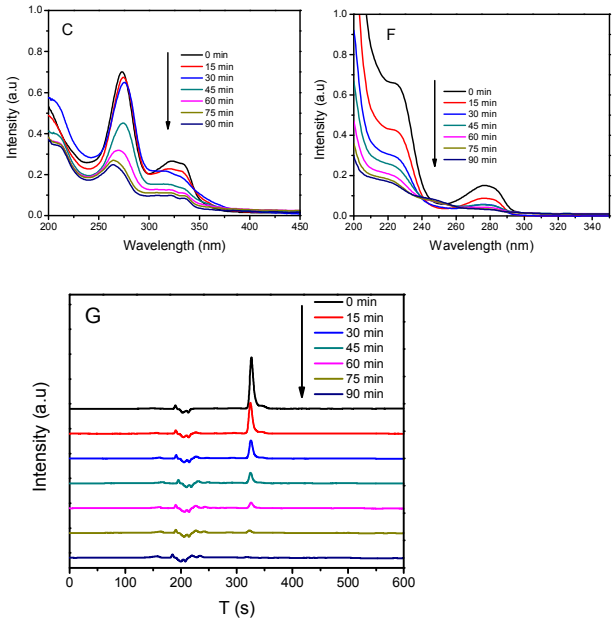

Fig. 8 Evolution of the absorption spectra of CIP (A) and BPA (D) without photocatalyst; CIP (B) and BPA (E) in the presence of $CoFe_2O_4$; CIP (C) and BPA (F) in the presence of Ag/AgCl/$CoFe_2O_4$ (3:1) under visible light irradiation. The HPLC of the BPA degraded solution for different time with the presence of Ag/AgCl/$CoFe_2O_4$ (3:1) (G).

3.6 Antibacterial activity

Fig. 9 A shows the results of antibacterial experiment of $CoFe_2O_4$ and Ag/AgCl/$CoFe_2O_4$ (3:1) in dark. It is clear that the $CoFe_2O_4$ has no inhibition zone while the Ag/AgCl/$CoFe_2O_4$ (3:1) has a clear inhibition zone about 19 mm against *E.coli*. The results indicate that the pure $CoFe_2O_4$ has no antibacterial ability while the Ag/AgCl/$CoFe_2O_4$ (3:1) has a good antibacterial ability in dark [34]. Fig. 9 B shows the results of photocatalytic antibacterial experiments. Without the existence of the photocatalyst, no obvious decrease of *E.coli* in amount was observed after the irradiation for 30 min. It indicates that the *E. coli* cannot be inhibited by the light irradiation. In the presence of pure $CoFe_2O_4$, lots of the *E.coli* was still alive after visible light irradiated for 30 min. No obvious decrease in amount was observed. It indicates that the pure $CoFe_2O_4$ has no significant ability in killing the *E.coli*. In the presence of Ag/AgCl/$CoFe_2O_4$ (3:1), lots of *E.coli* was still alive without light irradiation. However, when the system was irradiated by the visible light for 15 min, more than half of the *E.coli* was killed. When the system was irradiated for 30 min, all of the *E.coli* was killed. The results indicate that the Ag/AgCl/$CoFe_2O_4$ can be activated by the visible light to kill the *E.coli* efficiently. The results reveal that the Ag/AgCl/$CoFe_2O_4$ possesses the antibacterial ability with or without light.

Based on the above results, it can be concluded that the Ag/AgCl/$CoFe_2O_4$ is an effective and stable magnetic photocatalyst, which can degrade color and colorless pollutant as well as killing the bacteria in water at the same time. Besides, its magnetic property is benefit for its recovering after reaction. Thus, the Ag/AgCl/$CoFe_2O_4$ is a promising composite in practical fields during water process.

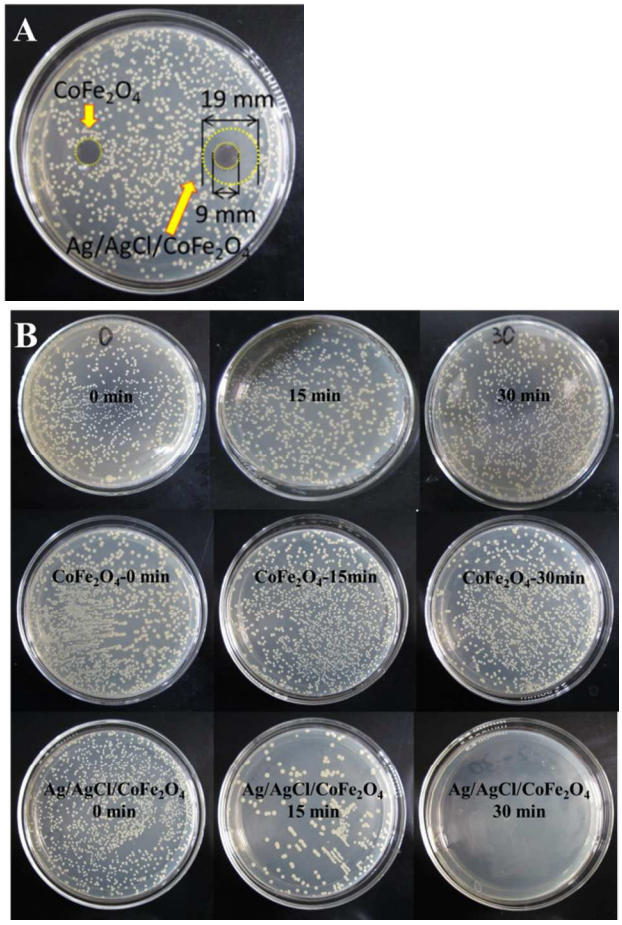

Fig. 9 The representative inhibition zone of $CoFe_2O_4$ and Ag/AgCl/$CoFe_2O_4$ (3:1) disks against *E. coli* after 24 h incubation in dark (A) and the photocatalytic antibacterial activities of light only, $CoFe_2O_4$ and Ag/AgCl/$CoFe_2O_4$ (3:1) against bacteria *E. coli* at different irradiation time (B).

Conclusions

The magnetic recoverable Ag/AgCl/$CoFe_2O_4$ photocatalyst has been successfully fabricated by a two-step method. The composite showed high degradation ability in degrading MO, CIP and BPA pollutants. The HPLC results showed that the BPA can be completely decomposed by the Ag/AgCl/$CoFe_2O_4$ (3:1) in 90 min. The combination of the Ag/AgCl and $CoFe_2O_4$ is so strong that the composite can be easily recovered by magnet after three cycle experiments and still kept the high photoactivity. Besides, the Ag/AgCl/$CoFe_2O_4$ showed high photocatalytic antibacterial ability against *E. coli*. This work provides a new strategy to synthesize magnetic recoverable photocatalyst.

Acknowledgements

This work is financially supported by the National Natural Science Foundation of China for Youths (No. 21407065), Natural Science Foundation of Jiangsu Province for Youths (BK20140533), China Postdoctoral Science Foundation (No.: 2014M551520, 2014M560399), Jiangsu Postdoctoral Science Foundation (1401143C), Jiangsu University Scientific Research Funding (No. 14JDG052).

Notes and references

[a] *School of Chemistry and Chemical Engineering, Jiangsu University, 301 Xuefu Road, Zhenjiang, 212013, P R China*
[b] *School of Energy and Power Engineering, Jiangsu University, 301 Xuefu Road, Zhenjiang, 212013, P R China*
[c] *School of Pharmacy, Jiangsu University, 301 Xuefu Road, Zhenjiang, 212013, P R China*

[1] H. X. Shi, G.S. Li, H. W. Sun, T. C. An, H. J. Zhao, P. K. Wong, *Appl. Catal. B: Environ.*, 2014, **158–159,** 301–307.
[2] H. Tong, S.X. Ouyang, Y. P. Bi, N. Umezawa, M. Oshikiri, J. H. Ye, *Adv. Mater.,* 2012, **24**, 229-251.
[3] W. B. Hou, S.B. Cronin, *Adv. Funct. Mater.,* 2013, **23**, 1612-1619.
[4] Z. Z. Lou, Z. Y. Wang, B. B. Huang, Y. Dai, *ChemCatChem***,** 2014, **6**, 2456-2476.
[5] J. G. McEvoy, Z. S. Zhang, *J. Photochem. Photobiol., C,* 2014, **19,** 62-75.
[6] P. Wang, B. B. Huang, X. Y. Qin, X. Y. Zhang, Y. Dai, J. Y. Wei, M. H. Whangbo, *Angew. Chem. Int. Ed.***,** 2008, **47**, 7931-7933.
[7] P. Wang, B. B. Huang, X. Y. Zhang, X. Y. Qin, H. Jin, Y. Dai, Z. Wang, J. Y. Wei, J. Zhan, S. Wang, J. Wang, M. H. Whangbo, *Chem. Eur. J.***,** 2009, **15**, 1821-1824.
[8] C. H. An, S. Peng, Y. G. Sun, *Adv. Mater.,* 2010, **22**, 2570-2574.
[9] H. S. Lee, J. E. Kim, T. Y. Kim, K. S. Suh, *J. Alloys Comp.,* 2015, **621**, 378-382.
[10] P. Wang, B. B. Huang, Q. Zhang, X. Y. Zhang, X. Y. Qin, Y. Dai, J. Zhan, J. Yu, H. Liu, Z. Z. Lou, *Chem. Eur. J.,* 2010,**16**, 10042-10047.
[11] P. Wang, B. B. Huang, Z. Z. Lou, X. Y. Zhang, X. Y. Qin, Y. Dai, Z. K. Zheng, X. N. Wang, *Chem. Eur. J.,* 2010, **16**, 538-544.
[12] H. G. Yu, L. L. Xu, P. Wang, X. F. Wang, J. G. Yu, *Appl. Catal. B-Envir.,* 2014, **144**, 75-82.
[13] Y. P. Bi, J. H. Ye, *Chem. Commun.,* 2009, **655**, 6551-6553.
[14] Y. Y. Li, Y. Ding, *J. Phys. Chem. C,* 2010, **114**, 3175-3179.
[15] Y. X. Tang, Z. L. Jiang, G. C. Xing, A. R. Li, P. D. Kanhere, Y. Y. Zhang, T. C. Sum, S. Z. Li, X. D. Chen, Z. L. Dong, Z. Chen, *Adv. Funct. Mater.,* 2013, **23**, 2932-2940.
[16] R. F. Dong , B. Z. Tian, C. Y. Zeng , T. Y. Li, T. T. Wang , J. L. Zhang, *J. Phys. Chem. C,* **2013,** ***117,*** 213-220.
[17] Y. S. Xu, W. D. Zhang, *ChemCatChem,* 2013, **5,** 2343–2351.
[18] Y. G. Xu, H. Xu, H. M. Li, J. X. Xia, C. T. Liu, L. Liu, *J. Alloys Comp.*, 2011, **509,** 3286–3292.
[19] W. S. Wang, H. Du, R. X. Wang, T. Wen, A. W. Xu**,** *Nanoscale***,** 2013,**5**, 3315-3321.
[20] J. F. Guo, B. W. Ma, A. Y. Yin, K. N. Fan, W. L. Dai, *Appl. Catal. B-Envir.,* 2011, **101**, 580-586.
[21] C. H. An, X. J. Ming, J. Z. Wang, S. T. Wang, *J. Mater. Chem.,* 2012, **22**, 5171-5176.
[22] B. Z. Tian, T. T. Wang, R. F. Dong, S. Y. Bao, F. Yang, J. L. Zhang, *Appl. Catal. B-Envir.,* 2014, **147**, 22-28.
[23] C. Y. Wang, L. Y. Zhu, C. Chang, Y. Fu, X. L. Chu, *Catal. Commun.,* 2013, **37**, 92-95.
[24] H. A. J. L. Mourão, A. Malagutti, C. Ribeiro, *Appl. Catal. A-Gen.,* 2010, **382**, 284-292.

[25] K. K. Senapati, C. Borgohain, P. Phukan, *Catal. Sci. Technol.,* 2012, **2**, 2361-2366.
[26] P. Sathishkumar, N. Pugazhenthirana, R. V. Mangalaraja, A. M. Asiric, S. Anandan, *J. Hazard. Mater.,* 2013, **252-253**, 171-179.
[27] P. Sathishkumar, R. V. Mangalaraja,, S. Anandan, M. Ashokkumar, *Chem. Eng. J.,* 2013, **220**, 302-310.
[28] S. Akbayraka, M. Kayab, M. Volkana, S. Özkar, *Appl. Catal. B-Envir.,* 2014, **147**, 387-393.
[29] L. J. Xu, W. Chu, Lu Gan, *Chem. Eur. J.,* 2015, **263,** 435-443.
[30] J. Deng, Y. S. Shao, N. Y. Gao, C. Q. Tan, S. Q. Zhou, X. H. Hu, *J. Hazard. Mater.,* 2013, **262**, 836-844.
[31] N. W. Li, M. B Zheng, X. F. Chang, G. B. Ji, H. L. Lu, L. P. Xue, L. J. Pan, J. M. Cao, *J. Solid State Chem.*, 2011, **184**, 953-958.
[32] W. Y. Bian, Z. R. Yang, P. Strasser, R. Z. Yang, *J. Power Sources,* 2014, **250**, 196-203.
[33] Y. G. Xu, H. Xu, H. M. Li, J. Yan, J. X. Xia, S. Yin, Q. Zhang. *Colloids Surf., A* , 2013, **416**, 80-85.
[34] J. X. Shu, Z. H. Wang, G. Q. Xia, Y. Y. Zheng, L. H. Yang, W. Zhang, Chem. Eng. J., 2014, **252,** 374-381.
[35] Y. H. Liang, S. L. Lin, L. Liu, J. S. Hu, W. Q. Cui, Appl. Catal. B., 2015, **164,** 192-203.
[36] S. G. Chen, Y. J. Guo, H. Q. Zhong, S. J. Chen, J. N. Li, Z. C. Ge, J.N. Tang, *Chem. Eng. J.,* 2014, **256**, 238-246.